Wideband MIMO channel sounder: capacity and spatial correlation under 2.4- and 5.2-GHz co-located conditions

B.T. Maharaj, *MIEEE,* J.W. Wallace, *MIEEE* and *L.P. Linde, SMIEEE*

***Abstract*— Due to complicated behavior of multiple-input-multiple-output (MIMO) wireless channels, direct measurement is currently the only viable option for accurate characterization. We present our cost effective, wideband MIMO channel sounder, capable of performing measurements with up to 8 transmit and 8 receive elements over 80MHz of instantaneous system bandwidth. This switched architecture system is similar to commercial channel sounders except at a much more modest cost. Channel capacity measurements at 2.4 and 5.2 GHz using a uniform linear array (ULA) are presented. Frequency scaling refers to the ability of measurements taken at one center frequency to predict those taken at a different frequency. An almost linear relationship exists between measured decorrelation for the ULA at the two distinct carrier frequencies, suggesting that the multi-path scattering behavior is very similar at 2.4 and 5.2 GHz for this indoor environment.**

***Index Terms*—multiple-input-multiple-output systems, MIMO.**

I. Introduction

The challenges of higher spectral efficiency, quality-of-service, and data rates in wireless systems have stimulated research in multiple antenna arrays for mobile and fixed wireless communication systems. Telatar [1] demonstrated that employing multiple antennas at both transmit (TX) and receive (RX) significantly increases the channel capacity in a multi-path environment, without increasing the system bandwidth or transmit power. These multiple-input multiple-output (MIMO) systems are good candidates for next generation wideband and ultra-wideband wireless local area networks.

The performance gains of MIMO systems have been explored by theoretical studies involving stochastic channel models [2], geometrical channel models [3], and direct channel measurement [4-7]. These studies demonstrate the high potential for increased performance, which can be realized by exploiting the multi-path structure of the channel with advanced space-time coding techniques [8]. While there may be extensive information concerning the behavior of antenna diversity in multipath channels [9], new issues have risen with respect to MIMO communications and the impact of antenna properties and it's configurations.

Design and assessment of MIMO systems employing sophisticated coding, modulation, and antenna arrays requires accurate characterization of the propagation channel. Such channel descriptions are possible through advanced modeling strategies or direct measurement. A number of MIMO channel models have been proposed, ranging from simple statistical models to advanced ray-tracing techniques [2-3,10-11]. Although channel models allow inexpensive implementation on computers, even the most advanced modeling strategies have failed to represent real channels with high accuracy. On the other hand, direct channel measurement [12-14] provides very accurate characterization, but such campaigns are both time consuming and expensive, allowing only a small set of communication channels to be investigated.

In this paper, we present an overview of the wideband channel sounder developed at University of Pretoria. We also present measured capacities for the uniform linear array (ULA) implementation and compare the capacities at 2.4 and 5.2 GHz for the same physical locations. We ale explore spatial correlation at a center frequency of 2.4 GHz to predict measurements at a much higher center frequency of 5.2 GHz, which we refer to as *frequency scaling*. Also, frequency scaling suggests that MIMO techniques employed in a system with one center frequency will be directly applicable to systems operating at other frequencies, possibly decreasing the development time of MIMO systems, network planning, etc.

This paper is organized as follows: Section II describes the measurement system and the environment while Section III explains the data processing aspects such as capacity and correlation calculations after the measurement campaign. Section IV presents the results using the ULA and finally Section V concludes the paper.

This work was supported by the National Research Foundation (NRF), through GUN 2053857.

B.T. Maharaj is with the Department of Electrical, Electronic and Computer Engineering, University of Pretoria, Lynnwood Road, Pretoria, South Africa, 0002 (telephone: 012-420 4636, fax: 012 – 362 5000, e-mail: {sunil.maharaj@up.ac.za}). Dr J.W. Wallace is with the Department of Electrical and Computer Engineering, Brigham Young University, Provo, UT84602, USA (e-mail: {wall@ieee.org }).

II. MEASUREMENT SYSTEM

A. Measurement Setup

Fig.1 depicts the transmit (TX) side of the channel probing system. The flexibility of the system allows the channel to be probed with arbitrary baseband signals (chirps, PRN sequences, etc.) For simplicity, we excited the channel with a repetitive multi-tone baseband signal that is mixed with the carrier frequency, generated very easily with a Rhode & Schwarz SMU200 vector signal generator. The multi-tone signal is of the form

$$x(t) = \sum_{i=0}^{N} \cos(2\pi f_i t + \varphi_i) \quad (1)$$

where

$f_i = (0.5 + i)MHz$

$i = 0,1,...,39$

$\varphi_i = \{0, \pi\}$

and φ_i is random (but fixed) phase shift for each tone that spreads the signal energy in time. To avoid artifacts associated with turning the signal on and off abruptly, the multitone signal of length T is multiplied by a Gaussian windowing function of the form

$$w(t) = \begin{cases} e^{-(T_1 - t)^2 / 2\sigma^2}, & 0 \le t < T_1 \\ e^{-(T_2 - t)^2 / 2\sigma^2}, & T_2 < t \le T \\ 1, & Otherwise \end{cases} \quad (2)$$

where T_1 and T_2 are the limits of the window, and the standard deviation σ controls the rise and fall time of the window. After power amplification, the windowed multitone signal is fed to a broadband microwave PIN diode (SP8T) switch, which routes the signal to one of N_T output antennas. The output power of the signal generator was adjusted to obtain a peak output power of 27 dBm.

Synchronization is achieved with highly stable 10MHz rubidium oscillators at TX and RX, whose careful calibration is critical to ensure negligible drift of relative TX/RX timing. RF sources were also phase locked to the rubidium references to ensure minimal frequency offset and drift. A custom designed synchronization (SYNC) unit provides all necessary triggering at TX and RX. This unit accepts the 10 MHz input reference and produces a trigger pulse on EVT1 every Q clocks and on EVT2 for every $Q \cdot N$ clocks, where N is the number of antennas. The unit also generates TTL switch signals that enable a new antenna every Q clocks. The TX/RX timing units are initially synchronized with a simple reset switch connected simultaneously to both units.

For the transmitter Q_T was set to 200 to give 20 μs of dwell-time for each transmit antenna. Combined with the Gaussian window, the channel is excited for approximately 15 μs on each antenna. Since there are N_T=8 transmit antennas, a complete scan of the array requires 160 μs. Also EVT1 is connected to the trigger input of the signal generator to ensure that the baseband signal waveform begins at the correct time instant.

Fig.2 depicts the receive system, where a SP8T switch routes the incoming signal from one of the N_R receive antennas to the receive RF chain. This signal is amplified by 40 dB though a low noise amplifier (LNA) having a noise figure (NF) of 3.5 dB, down-converted to a 50 MHz intermediate frequency (IF), filtered, and sampled at 500 Msamples/s through Channel1 of the high speed data acquisition card. Channel2 of the same card acquired the 10 MHz reference to allow accurate re-sampling of the received waveforms to ensure complete phase-coherence of the system.

At the receiver, Q_R was set to 1600, thus causing a single transmit antenna switch for each complete scan of the transmit array. With N_R=8 receive antennas, a complete scan of the MIMO channel required 1.28 ms. EVT2 of the receive SYNC unit is attached to the trigger of the acquisition card, ensuring that sampling is performed over the correct window of time.

The wideband MIMO channel response $\mathbf{H}(\omega)$ for the jth TX and ith RX is computed at K=80 discrete frequency bins by dividing the FFT of the measured signal on the jth TX and ith RX timeslot by the FFT of the known transmit waveform and selecting bins corresponding to the tones. Proper choice of the waveform length ensures that each tone frequency coincides with a single FFT bin.

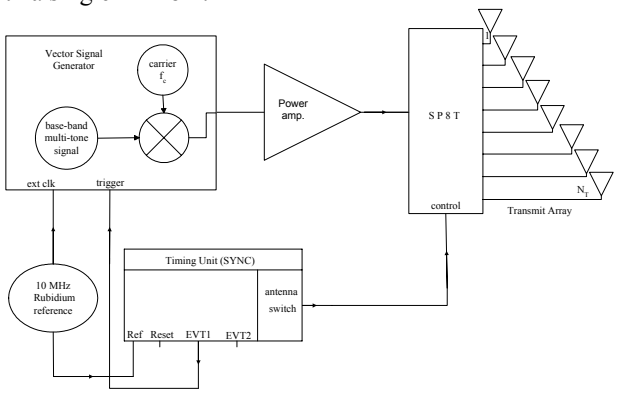

Fig. 1 TX system diagram of WB MIMO channel sounder

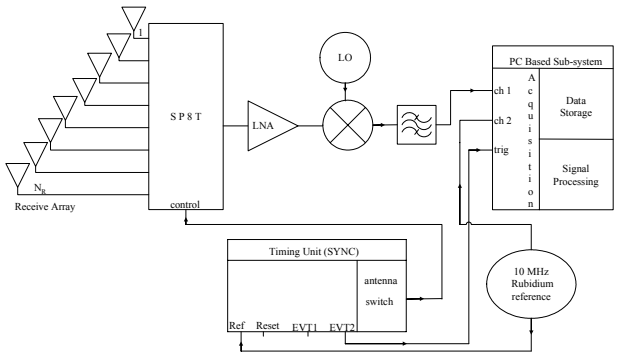

Fig. 2 RX system diagram of WB MIMO channel sounder

B. Measurement Environment

The measurements reported herein, as shown in Fig. 3, were carried out in the offices and laboratories at the Carl Emily Fuchs Institute of Microelectronic (CEFIM) in the Department of Electrical, Electronic and Computer Engineering at the

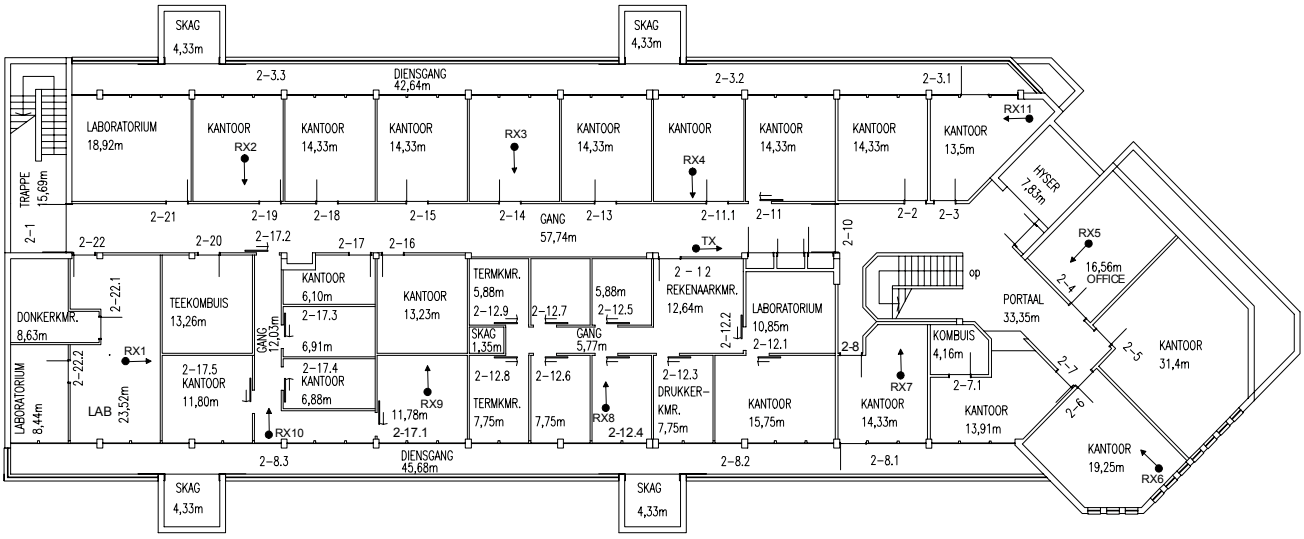

Fig. 3 Measurement campaign locations with TX and RX positions in CEFIM at UP

University of Pretoria (UP), South Africa. TX was located at the same fixed position in the corridor, while the RX antenna was located in 11 different adjoining offices and laboratories. Vertically polarized monopole arrays with λ/2 inter-element spacing was used at 5.2 GHz while a 0.3λ inter-element spacing was used at 2.4 GHz. This was due to the large size of the linear dipole array on our uniquely designed virtual array grid. The internal structure of the building is largely comprised of dry wall partitioning with concrete pillar support. The locations would sufficiently resemble a rich scattering environment with wood, metallic, plants, persons and fabric make up.

III. Data Processing

If the system response is known, its effect can be removed from the measured channel matrices by simple division, which process we refer to as system calibration. The system response is characterized by measuring (1) the insertion loss and phase of the SP8T switches for all 8 ports and (2) the combined response of the TX and RX RF chains when excited with the channel probing signal.

The SP8T insertion loss and phase were measured for all eight ports on a network analyzer. The combined effect of the baseband signal and TX and RX RF chains is obtained by connecting the output of the TX RF chain through the appropriate attenuators directly to the input of the receive RF chain. Since we employed an IF variable gain amplifier (VGA) that had slightly different frequency response for the various gain levels, the chain response was measured for each allowed gain level ranging from 0 to 40 dB in 5 dB steps.

At each of the 11 locations, 20 channel snapshots were recorded with 200 ms between snapshots. This results in a 4-s acquisition time, and since the channel sounding was for a fixed TX and RX case, negligible channel variation was observed across this duration.

To remove the effect of path loss in our computations, channel matrices were normalized according to

$$\widetilde{\mathbf{H}}^{(n)} = \left(\frac{1}{N_R N_T N_S} \sum_{m=1}^{N_S} \left\| \mathbf{H}^{(m)} \right\|_F^2 \right)^{-1/2} \mathbf{H}^{(n)}, \tag{3}$$

where $\widetilde{\mathbf{H}}^{(n)}$ and $\mathbf{H}^{(n)}$ are the n^{th} normalized and un-normalized channel matrices, respectively. N_s is the number of channel measurements (snapshots and frequency bins) at a single location, and $\|\cdot\|_F$ is the Frobenius norm.

For the ULA, the channel capacity for each frequency bin is computed according to the uninformed transmit capacity from [2] as

$$C = \log_2 \det(I + \frac{\rho}{N_T} \widetilde{\mathrm{H}} \widetilde{\mathrm{H}}^H), \tag{4}$$

where I is the 8x8 identity matrix, ρ is an assumed average SISO signal to noise ratio (SNR), N_T is the number of TX antennas, $\widetilde{\mathrm{H}}$ is the normalized channel matrix, and $(.)^H$ is the conjugate matrix transpose. The average capacity across all 80 frequency bins for location loc is denoted $\overline{C}_{\mathrm{loc}}$.

The ULA measurements, on the other hand, are well suited for correlation studies, since the ULA has a shift-invariant correlation structure under the assumption of far-field scattering. Also, in a rich multi-path environment, the correlation of the ULA will depend mainly on the relative orientation of the array and the multi-path, allowing the directional signature of the multi-path to be investigated.

For the ULA, far-field scattering produces a shift-invariant correlation structure, allowing transmit or receive correlation to be written as a function of just the offset between elements, instead of a function of both indices. In this case, the shift-invariant correlation coefficient at the RX with an element displacement of ℓ is

$$\rho_\ell = \frac{\left[\sum_{k=1}^{N_S}\sum_{j=1}^{N_T}\sum_{i=1}^{N_R-\ell} H_{i,j}^{(k)} H_{i+\ell,j}^{(k)*}\right]}{\left[\left(\sum_{k=1}^{N_S}\sum_{j=1}^{N_T}\sum_{i=1}^{N_R-\ell}\left|H_{i,j}^{(k)}\right|^2\right)\left(\sum_{k=1}^{N_S}\sum_{j=1}^{N_T}\sum_{i=1}^{N_R-\ell}\left|H_{i+\ell,j}^{(k)}\right|^2\right)\right]^{1/2}}, \quad (5)$$

where N_s=20*80 is the number of snapshots taken across all frequency bins and observations, N_T=8 and N_R=8 are the number of transmit and receive antennas, respectively, and $H_{i,j}^{(k)}$ is the k^{th} channel snapshot from the j^{th} TX to the i^{th} RX antenna. Similarly the shift-invariant TX correlation is computed by interchanging roles of TX and RX in (5).

To simplify the analysis of correlation, we model the magnitude of ρ_ℓ with the exponential function

$$y_\ell = e^{-b\ell\Delta x}, \quad (6)$$

where Δx is the element separation in wavelengths, and b is the estimated *decorrelation* parameter, which is chosen to minimize the average mean square error (MSE) $\bar{d}$ at {TX, RX}, where

$$\bar{d} = \frac{1}{\{N_T, N_R\}} \sum_{\ell=0}^{\{N_T,N_R\}-1} (|\rho_\ell| - y_\ell)^2 . \quad (7)$$

Separate values of b are estimated at TX and RX for each frequency.

Frequency scaling of capacity and correlation is tested by applying a simple linear regression of either the capacity or decorrelation at the two frequencies, or

$$q_{5.2} = a_1 + a_2 q_{2.4}, \quad (8)$$

where $q_{\{5.2,2.4\}}$ is the decorrelation parameter at 5.2 GHz and 2.4 GHz, respectively, and a_1 and a_2 are obtained with a minimum MSE fit.

IV. Results

Using (4), and assuming a target system SNR of 20 dB, the ULA capacity across the 80MHz excitation bandwidth for each of the 11 locations was calculated and averaged as shown for location 3 in figure 4. Figure 5 shows the comparison of the average capacity, $\bar{C}_{loc}$ for all the measured locations at both the centre frequencies. One observes that in most cases the capacity at 5.2 GHz is slightly larger than that at 2.4 GHz, most likely due to more scattering due to the smaller wavelength.

Next, we study the impact of frequency scaling on the correlation present in the ULA data. Figure 6 plots the shift-invariant correlation coefficient at location 4 versus antenna element displacement (in wavelengths) with respect to the RX, for both 2.4 GHz and 5.2 GHz, where the symbols and smooth lines refer to data points and the best-fit exponential model, respectively. A similar tendency prevailed with respect to the TX at location 8 as shown in fig. 7 while similar plots were found for most of the other TX, RX locations.

TABLE I
Decorrelation parameter (b) and error wrt wavelength (λ) at RX

Locations	5.2 GHz		2.4 GHz	
	b	error (%)	b	error (%)
1	0.8702	3.27	0.8690	4.76
2	1.2795	1.76	1.0903	4.48
3	1.5591	5.64	1.2546	2.00
4	0.2550	1.06	0.4080	0.75
5	1.0536	2.57	0.8799	3.49
6	0.3432	0.98	0.3182	1.15
7	0.9071	0.72	0.9978	0.17
8	0.4883	1.46	0.4190	0.35
9	0.3442	0.45	1.2042	1.18
10	1.0403	2.40	0.9980	2.90
11	1.9721	5.41	1.5548	3.65

TABLE II
Decorrelation parameter (b) and error wrt wavelength (λ) at TX

Locations	5.2 GHz		2.4 GHz	
	b	error (%)	b	error (%)
1	0.9769	1.54	0.9511	0.18
2	1.0189	2.66	0.8849	1.69
3	1.2988	1.68	1.0666	2.34
4	0.2400	2.96	0.4270	2.90
5	0.8746	2.08	0.8325	0.06
6	0.7402	5.84	0.6833	0.56
7	1.4634	1.13	1.2678	1.38
8	0.2845	0.51	0.4302	0.84
9	0.3530	1.03	1.6701	0.96
10	1.0134	0.75	1.4210	3.15
11	0.9514	0.49	1.0462	0.76

The RX decorrelation parameter b, as well as the MSE of the model fit to the data points for all 11 locations is computed as shown in Table I for both the 5.2 GHz and 2.4 GHz channel data. Typical MSE of the model is between 0.2% and 3.3% with only about 20% of the locations having an error above 4%. Average error for the 5.2 GHz and 2.4 GHz sets is 2.34% and 2.26%, respectively, indicating remarkably good fit considering the simplicity of the model.

Following this same procedure for TX correlation, results in the decorrelation parameter values listed in Table II. Typical MSE of the model is between 0.2% and 2.9%. Average error for the 5.2 GHz and 2.4 GHz sets is 1.9% and 1.4%, again indicating good fit. The cross correlation between the capacity and the decorrelation parameter, b for the ULA shown in Table III. The average obtained is 82%.

TABLE III
Cross correlation of capacity (C) and decorrelation parameter (b)

	2.4 GHz		5.2 GHz	
	TX	RX	TX	RX
%	84	89	75	81

This confirms and validates that there should be a strong dependence [12] between the capacity and the de-correlation parameter as determined in our model.

To establish the effect of frequency scaling on the decorrelation, Figure 8 plots the TX parameter $b_{5.2}$ versus $b_{2.4}$ as in Table II. One observes that there is very high dependence present with the exception of location 9 (0.3530,1.6701). The broken and solid lines in Figure 8 show the linear regression of the data when all data points

are considered and when location 9 is discarded as an outlier, respectively. MSE values for these two cases are 0.136 and 0.038, respectively. Similarly, performing a linear regression of the decorrelation parameter at RX, results in MSE values of 0.109 and 0.014, when again location 9 is included and discarded, respectively. These results show that the correlation at the two frequencies exhibits a strong dependence, suggesting that not only the level of multi-path at the two frequencies is similar, but also the directional signature is related.

V. CONCLUSION

This paper has presented Africa's first cost effective wideband MIMO channel sounder, the capacity obtainable using a ULA at 2.4 and 5.2 GHz for exactly the same locations and the study of the effect of frequency scaling on correlation in MIMO wireless systems. Measured capacity for the ULA at 2.4 GHz and 5.2 GHz suggests that one could expect a higher data rate at the higher centre frequency for this indoor environment. A linear dependence was found for correlation obtained from ULA measurements at the same two center frequencies, suggesting high correlation in the directional signature of the multi-path propagation. These results indicate that propagation mechanisms in the indoor environment at these two distinct carrier frequencies may be very similar, leading to possible cost savings in channel measurement campaigns, network planning, and MIMO system development.

REFERENCES

[1] I. E. Telatar, "Capacity of multi-antenna Gaussian Channels," Technical Report #BL0112170-950615-07TM, AT&T Bell Laboratories, 1995.

[2] G. J. Foschini and M. J. Gans, "On limits of wireless communications in a fading environment when using multiple antennas," *Wireless Personal Communications*, vol. 6, no. 3, pp. 311 – 335, Kluwer Academic Publishers, March 1998.

[3] B.T. Maharaj and L.P. Linde, "Capacity for Spatial-Temporal Correlated MIMO Fading Channel," *in Proc. IEEE Africon 2004*, pp. 269-274, September 2004.

[4] J.W. Wallace, M.A. Jensen, A.L. Swindelhurst and B.J. Jeffs, "Experimental Characterization of the MIMO Wireless Channel: Data Acquisition and Analysis," *IEEE Trans. on Wireless Comms*., vol. 2, no. 2, pp. 335-343, March 2003.

[5] D. Gesbert, H. Bolcskei, D. Gore and A. Paulraj, "MIMO wireless channels: Capacity and Performance prediction," *Proceedings of IEEE Globecom Conference*, vol. 2, pp. 1083-1088, November 2000.

[6] H. Ozcelik, M. Heredin, H. Hofsetter, E. Bonek, "A comparison of measured 8X8 MIMO systems with a popular stochastic channel model at 5.2 GHz," *in Proc. ICT'2003*, March 2003.

[7] M. Herdin, H. Ozcelik, H. Hofsetter and E. Bonek, "Variation of measured indoor MIMO capacity with receive direction and position at 5.2 GHz", *Electronics Letters*, 38(21), pp. 1283-1285, 2002.

[8] V. Tarokh, N. Seshadri and A.R. Calderbank, "Space-time codes for high data rate wireless communication: Performance criterion and code construction," *IEEE Trans. Inform. Theory*, vol. 44, pp. 744-765, March 1998.

[9] W.C. Jakes, *Microwave Mobile Communications*. Piscataway, NJ: IEEE Press, 1993.

[10] Ali Abdi, Mostafa Kaveh, "A Space-Time Correlation Model for Multielement Antenna Systems in Mobile Fading Channels," *IEEE J. on Selected Areas in Comms.*, vol. 20, no. 3, pp. 550-560, April 2002.

[11] G.J. Byers and F. Takawira, "The Influence of Spatial and Temporal Correlation on the Capacity of MIMO Channels," *in Proc. IEEE WCNC 2003*, vol. 1, pp. 359 – 364, March 2003.

[12] M.A. Jensen and J.W. Wallace, "A review of antennas and propagation for MIMO wireless communications," *IEEE Trans. Antennas and Propag*., vol. 52, pp. 2810-2824, Nov. 2004.

[13] B.T. Maharaj, L.P. Linde, J.W. Wallace and M.A. Jensen, "A cost effective wideband MIMO channel sounder and initial co-located 2.4GHz and 5.2GHz measurements", *in Proc. IEEE ICASSP*, vol.3, Philadelphia, pp. 981-984, March 2005.

[14] B.T. Maharaj, J.W. Wallace, L.P. Linde and M.A. Jensen, "Linear dependence of double-directional spatial power spectra at 2.4 and 5.2 GHz from indoor MIMO channel measurements" *IEE Electronic Letters*, 41(24), pp. 1388-1340, November 2005.

B.T. Maharaj (Sunil) (MIEEE 2006, MSAIEE 1997) received both his BSc Eng. and MSc Eng. in Electronic Engineering from University of Natal, South Africa. He also holds a MSc with Merit in Operational Telecommunications (1996) from University of Coventry, UK.

He worked for three years at Electromagnetic Laboratory Pty Ltd as a microwave design engineer. He subsequently worked for about eight years at the Eastern Cape Technikon and is Acting Head: SENTECH Chair in Broadband Wireless Multimedia Communications (BWMC) in the Department of Electrical, Electronic and Computer Engineering, University of Pretoria, South Africa. Mr Maharaj is currently completing his PhD at University of Pretoria and his research interests are in software defined radios (SDR), MIMO systems channel modeling and microwave component design.

J.W. Wallace (Jon) (S'99-M'03) received the B.S. (summa cum laude) and PhD degrees in electrical engineering from Brigham Young University (BYU), Provo, UT, in 1997 and 2002 respectively.

From 1995 to 1997, he worked as an Associate of Novell, Incorporated, Provo, UT. During 1997, he was a Member of the Technical Staff for Lucent Technologies, Denver, CO. From 1998 to 2002, he worked as a graduate student researcher in the BYU Wireless Communications Laboratory where he is currently a Research Associate. From 2002 to 2003, he visited the Technical University of Vienna Mobile Communications Group. His research interests include wireless channel sounding and modeling, optical device modeling and remote sensing.
Dr Wallace received the National Science foundation Graduate Fellowship in 1999 and the Harold A. Wheeler Applications Prize Paper Award in the IEEE Transactions on Antennas and Propagation in 2002.

L.P. Linde holds a Hons-BEng(1973) degree in Electrotechnical Engineering from the University of Stellenbosch and M.Eng (1980) and D.Eng (1983) degrees in Electronic Engineering from the University of Pretoria. He is a full professor and is presently the Group Head of Signal Processing and Telecommunications in the Department of Electrical, Electronic and Computer Engineering, University of Pretoria. He also holds the position of Director of the Centre for Radio and Digital Communications (CRDC) at University of Pretoria and Director of DigiMod Pty Ltd.

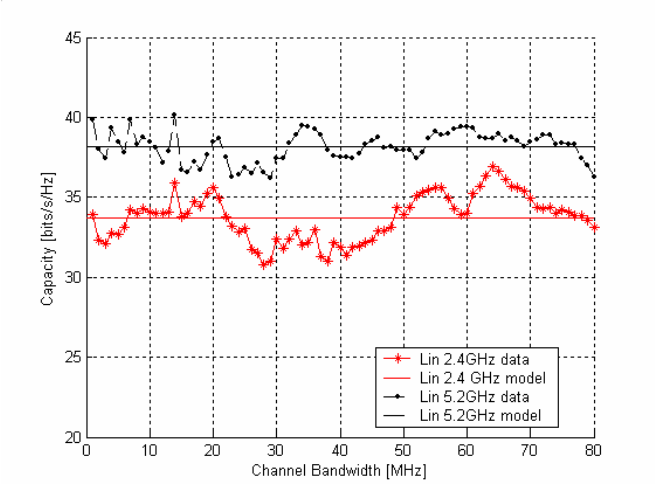

Fig. 4 Channel capacity versus excitation bandwidth for ULA at location 3

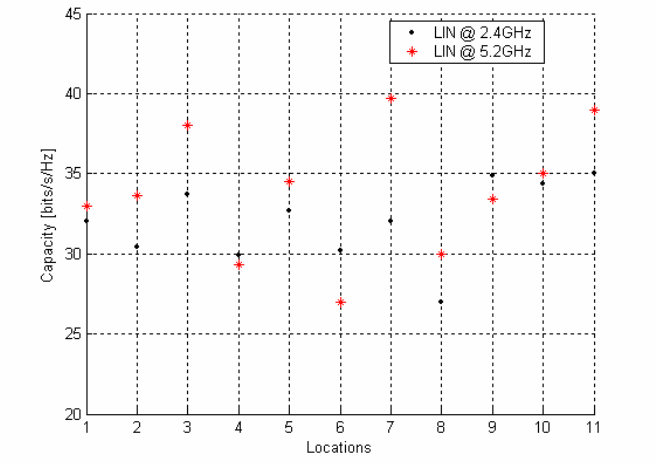

Fig. 5 Average channel capacity with ULA for each of locations in CEFIM

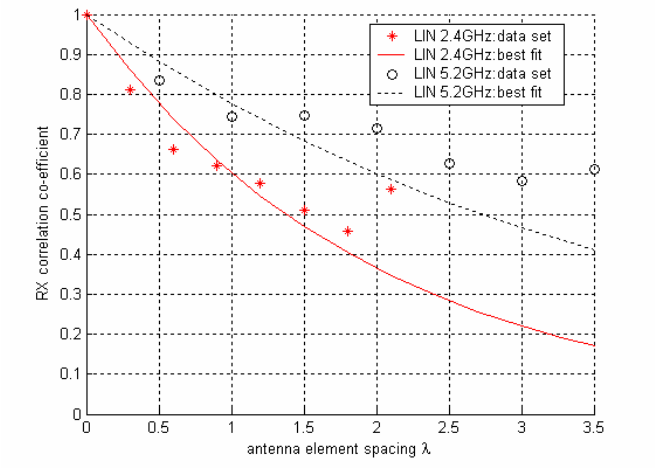

Fig. 6 Computed relative decorrelation coefficients with curve fit for RX at location 4

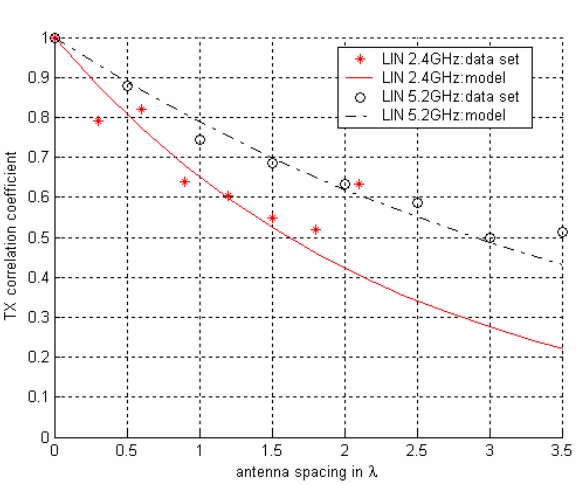

Fig. 7 Computed relative decorrelation coefficients with curve fit for TX at location 8

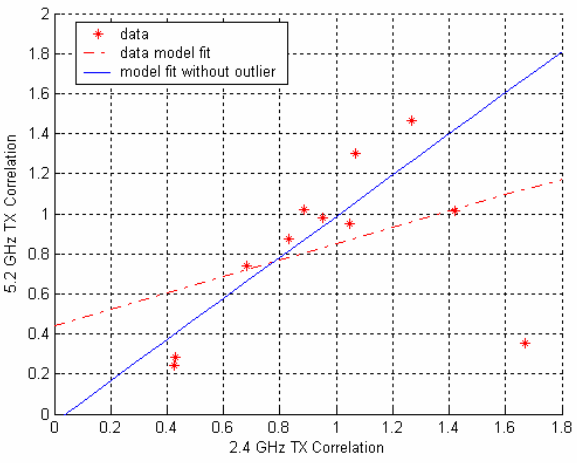

Fig. 8 Relationship of TX decorrelation with respect to frequency scaling